THE EFFECTS OF SWEEP AND BLUNTNESS ON GLANCING INTERACTIONS AT SUPERSONIC SPEEDS

ICAS-86-1.2.1

J.L. Stollery, N.R. Fomison and S. Hussain
College of Aeronautics
Cranfield, Bedford U.K.

Abstract

The glancing interaction between an oblique shock wave and a turbulent boundary layer has been studied experimentally using variable incidence fins mounted from the side wall of a supersonic wind tunnel. The separate and combined effects of incidence, bluntness and sweep were determined using 30 different models. The study includes surface oil flow pictures, taken over both the fin compression surface and the side-wall, and extensive side-wall pressure distributions. The results show the complex nature of the interaction, the strong effect of bluntness and the ameliorating effect of sweep.

I. Introduction

Glancing interaction is one of the most common forms of three-dimensional interference in which a body-generated shock wave cuts across the path of a boundary layer growing over an adjacent surface. An excellent review of the whole field of swept shock wave/boundary layer interaction has just been completed by Settles and Dolling[1]. Our experiments are an extension of those reported earlier by Kubota and Stollery[2] and now include the very important effects of bluntness and sweep. A three-dimensional fin was mounted from the side of a supersonic wind tunnel and the fin leading edge shock interacted with the thick turbulent boundary layer on the wall to give a rich variety of complex flows depending on the incidence, bluntness and sweep of the fin. The test results are relevant to wing-fuselage, fin-tailplane and various engine-intake geometries.

II. Experimental Details

The experiments were made in the College of Aeronautics continuous supersonic wind tunnel operating at a Mach number of 2.4. The tunnel reservoir pressure and temperature were 0.27 bar and about 300°K respectively. The test section Reynolds number per cm. was 3.1×10^4 and the fully developed turbulent boundary layer on the tunnel wall had a 99.5% thickness of 1.6 cm. The corresponding displacement and momentum thicknesses were 0.38 and 0.10 cm.

The experimental arrangement is shown in Fig. 1 and some of the models used are sketched in Fig. 2. A total of 30 fins were tested covering sweep angles from 0 to 75° and bluntess radii from 0 to 12.7 mm. The blunted models had semi-circular leading edges in the plane normal to the leading edge (i.e. elliptic in the freestream direction if the edge was swept). The sharp leading edge models were made from 5 mm thick plate chamfered on the 'expansion side' to give a nose angle of 15° measured normal to the leading edge (Fig. 2.)

Surface oil flow patterns were formed using a mixture of titanium dioxide and motor oil with a little oleic acid to avoid coagulation. The models were painted matt black to give the greatest photographic contrast.

When the fin leading edge is swept back the position of the shock wave without any interaction is unknown and either experiments or calculations must be made to find it. In our study two complete sets of delta wings were made with sharp and blunt leading edges respectively. Some of the blunt models are shown in Fig. 3. These were sting-mounted in the middle of the tunnel working section and photographed at M = 2.4 using a conventional single-pass schlieren system. Pictures were taken in both plan and elevation, the plan view was used to determine the 'tip effect' present. The flow patterns were recorded on high speed "Polaroid" black and white film rated at 3000 ASA. The pictures gave the shock wave position in the absence of the wall boundary layer and this shock wave is subsequently referred to here as the 'inviscid' shock, (Fig. 4).

Detailed surveys of the surface static pressure distribution in the interaction region were made by means of an array of pressure ports drilled in the turntable (Fig. 1). Each of the 220 ports were connected in turn by a scanivalve to a "Setra 239" differential pressure gauge. The ports were scanned slowly with up to one second being allowed for settling time. The signals from the pressure transducer were amplified, digitised and displayed using an on-line computer. The information was stored on floppy discs for later analysis. Twenty readings were taken for each port and the average recorded.

III Results and Discussion

Sharp, Unswept Fins

Previous investigations e.g. Ref. 2, have described in some detail the development of the glancing interaction flow pattern on the compression side of a wall-mounted, sharp, unswept fin. Fig. 5 shows the main flow features. Even at a fin incidence of 5° (Fig. 5a,) the disturbance caused by the oblique shock wave propagates well upstream through the boundary layer. The surface streamlines on the side wall begin to deflect and converge well ahead of the inviscid shock position. A small corner vortex develops as the high pressure air on the fin tries to 'escape' laterally, meets the side wall, separates from the fin surface and re-attaches on the side wall before flowing down-stream.

As the fin incidence is increased (Fig. 5b) so the wall surface streamlines deflect more violently and form a line of 'complete convergence'. We shall refer to this line as a separation line on the grounds that some streamlines originally close to the surface move away forming a flattened vortex, initially still within the boundary layer region (Fig. 5b). Pressure signatures taken parallel to the fin surface begin to show a plateau region as complete convergence develops (Fig. 6) which is reminiscent of the more easily defined

two-dimensional separation.

Incipient separation, the condition at which the boundary layer just separates, is never easy to define. It is particularly difficult in three dimensional flows since we are looking for the first appearance of a complete convergence line. Theoretically the surface flow pattern would show streamlines converging from both the upstream and downstream sides to form the characteristic herring-bone pattern. Unfortunately, if the vortex formed after separation is weak, and this is almost inevitably the case under incipient conditions then only the upstream surface flow lines are likely to be visibly convergent. Nevertheless it is always possible to define unseparated and well-separated flows and Kubota and Stollery[2] bracketed the incipient condition between these two as shown in Fig. 7. Also shown are the criteria of McCabe and Korkegi, which although they strictly determine when the surface flow has deflected sufficiently to lie parallel to the inviscid shock, the distinction may be a small one. Fig. 7 is important because it shows how relatively small fin-incidence angles (weak glancing shocks) can cause separation. For unswept interactions the turbulent boundary layer is capable of surviving much stronger shock waves without separating, (Fig. 8). For our Reynolds number based on boundary layer thickness of about 5×10^4 and our Mach number of 2.4 the two dimensional value of α_i according to Fig. 8, taken from the paper by Elfstrom[3], is about 18°. This compares with the value of α_i for glancing interaction at $M_\infty = 2.4$ as generated by a sharp unswept fin, of about 8°.

The Effects of Sweep, Sharp Leading-Edge

Sweep reduces the strength of the inviscid shock and although the root of the fin is never swept the oblique shock must weaken from the wedge value towards the cone value as the leading edge sweep is progressively increased.

This is shown in Fig. 9 where the shock wave angle measured at the root chord of a flat-plate-delta-wing with a sharp leading edge is plotted. At zero sweep the standard shock wave angles for a wedge are measured but as the sweep is increased so the shock angle is reduced. At $\Lambda = 75°$ the measured value is closer to that of a cone than that of a wedge. Because sweeping the fin leading-edge reduces the shock strength at a given incidence it will have a powerful effect on the whole interaction footprint area. Fig. 10 compares the isobar plots over the sidewall for swept and unswept fins at $\alpha = 13°$. The comparison is striking. Because the shock wave angle is smaller and the shock waker, the upstream influence is reduced. The overall pressure rise and the pressure levels throughout the interaction region are also reduced.

If the pressure distribution along a line parallel to the fin, or normal to the inviscid shock wave, is plotted, then the pressure distribution for the unswept fin has a plateau region in the vicinity of the shock. The oil flow picture shows a strong well defined convergence line and we have no hesitation in describing the flow as separated. However for the fin with 75° of sweep the pressure distribution rises smoothly throughout the interaction region and there is no clear sign of a plateau. Nevertheless, the oil flow pattern shows a thin but well defined convergence line and, among others, Settles and Lu[4] have shown this to be a good indicator of a 3D separated region. At the higher incidence $\alpha = 17°$, $\Lambda = 75°$ the isobars do show clear evidence of a plateau region.

Thus it would seem that $\alpha = 13°$, $\Lambda = 75°$ is close to the incipient separation condition. Settles and Lu[4] suggest an incipient separation criterion for swept fins of $\Theta - \mu_\infty = 3.5°$. At our Mach number of 2.4 the Mach angle μ_∞ is 24.6° so that $\Theta = 28.1°$. Fig. 9 then suggests that α_i is indeed around 13° for $\Lambda = 75°$.

What the criterion $\Theta - \mu_\infty = \text{const.}$ is saying is that for a given Mach number the shock wave angle, i.e. the shock strength, is the dominant factor. This seems intuitively sensible so that once again referring to Fig. 9 we can see that sweeping the fin leading edge is likely to increase α_i by about one degree for every twenty degrees of sweep. The oil flow patterns are consistent with this suggestion. At zero sweep α_i is about 8°, at 60° α_i is around 11° whilst at 75° of sweep α_i is close to, but below, 13° as already discussed.

The flow development for a sharp edged fin with moderate sweep (i.e. up to say 45° here) is similar to that for the unswept fin already discussed (see Fig. 5), the effect of sweep being to delay the incidence at which changes take place. Thus provided the fin leading edge is still supersonic the effect of sweep is roughly equivalent to a reduction in fin incidence. For large fin sweep angles and high incidence the geoemtry is exactly that of a vortex generator. The main features of the flow field will be similar to those sketched by Shen[5] for laminar low-speed flow (Fig. 11). However, in our case, the glancing interaction generates the primary vortex and, as already described, the flow below and around this primary vortex is complex and is not shown in Fig. 11. The flow over the compression side of a delta wing is also interesting. If the leading edge is supersonic and the incidence is small there are three flow attachment lines, one along the centreline and one on each of the leading edges to which the shock wave is attached. As the wing incidence is increased so the shock wave detaches and flow begins to 'spill' around the leading edge. The outer attachment lines move inboard and eventually coalesce on the centreline. The flow development is shown in Fig. 12 and further details can be found in the papers by Bertram et.al.[6] and by Stollery and Richards[7]. The flow features described above will be reflected in the oil flow pictures taken here on the fin; but the effect of the primary vortex, caused by the glancing interaction, will severely modify or even obscure them.

At high enough angles of sweep and incidence the fin leading edge shock will become detached, the leading edge will be subsonic and a strong leading edge vortex will form over the expansion side of the delta wing as shown in Fig. 11. In the tests reported here the fins swept 75° always had subsonic leading edges.

The Effects of Bluntness, Zero Sweep

Immediately leading edge bluntness is introduced there has to be a dramatic change because the shock wave is forced to detach and the two sides of the fin can communicate more easily. Part of the bow shock will be normal to the flow and will be so strong that local separation is inevitable. Local separation will, in turn, feed forward and modify the shape of the bow shock, creating a lamda-like foot. Some indication of the potential complexity can be gained from low speed flow. The bottom of any boundary layer must be subsonic and Fig. 13 shows the flow ahead of a circular cylinder protruding through a laminar boundary layer on a flat plate. Viewed from above, the obstacle generates a series of counter-rotating horseshoe vortices whose strength and size decreases with distance away from the body. As surmised, even when the mainstream is supersonic and the boundary layer turbulent the horseshoe vortices remain. Winkelmann[9] studied such a flow at $M_\infty = 5$ and some of his surface flow patterns are drawn in Fig. 14. The various separation and attachment lines on the wall are clearly visible. The pattern on the side of the fin is interesting because of a 'jet like' zone bounded on both sides by separation lines. This is caused by the pocket of gas near the root of the fin which has the highest stagnation pressure, (having been processed by two weaker shocks rather than one bow shock). This expands vigourously backwards around the shoulder of the fin and upwards towards the lower pressure zone. The tests by Fomison[10] display similar characteristics, his surface flow and vortex skeleton patterns are shown in Fig. 15.

The effect of bluntness on the pressure distributions is equally dramatic. Near the nose region pressure signatures taken parallel to the fin axis show a characteristic double peak, each peak being on an attachment line. Fig. 16 shows how, near the nose, the pressure is bluntness dominated but for large X/D the pressure asymptotes to the inviscid wedge value. Of course as the pressure survey is taken further and further away from the fin surface (i.e. large Y/D) so the signature reverts towards that for a sharp leading edged surface.

Two of Fomison's photographs taken at $\alpha = 15°$ emphasise how the surface flow pattern in the neighbourhood of the nose remains unchanged with incidence, (Fig. 16b).

The Combined Effects of Bluntness and Sweep

As mentioned earlier the shape of the leading edge becomes a more and more slender ellipse in the freestream direction as the sweep is increased; so the stand-off distance of the bow shock decreases rapidly (Fig. 17). This means that with a swept blunt fin on a wall, the upstream influence of the bow shock is reduced and all the previously noted effects of bluntness are muted and compressed into a smaller zone of interaction. Nevertheless many of the features are still identifiable as Fig. 18 shows for a blunt fin with 45° of sweep. A sketch of the surface flow pattern and a vortex skeleton representation of the flow are shown in Fig. 19.

The effect of sweep on the blunt fin pressure distributions is again dramatic. The pressure ratio p/p_∞ at the nose-root junction ($X_g = Y_g = Z_g = 0$) drops from 7.7 to 1.4 as the sweep increases from 0° to 75°. (The stagnation pressure ratio p_0/p_∞ at $M_\infty = 2.4$ is 8.7). Fig. 20 shows this effect and demonstrates how the pressure peak associated with the nodal point of attachment weakens and retreats towards the leading edge as the sweep is increased.

Of course it is not just the nose region that is influenced by sweep. Sweep weakens the bow shock and so reduces the magnitude of the interaction and hence the pressure levels throughout the whole flow field. One way of showing the overall effect is with an isometric sketch. Two of these are shown in Fig. 21 contrasting the surface pressure distributions for a blunt fin at zero sweep and incidence, with one swept back 30°.

The Unsteadiness of the Interaction

The boundary layer that the fin is disturbing is turbulent and hence, by definition, unsteady. Pressure measurements deliberately made using long tube connections between port and transducer will record 'steady' average values. The surface flow visualisation technique is not designed to indicate rapid fluctuations and the very sharpness of the pictures may induce forgetfulness of the turbulent nature of the flow. What is perhaps surprising is that in many complex turbulent and separated flows (including this one) there is no gross unsteadiness, no large movement of the shock positions or of the separation and re-attachment points.

In order to measure the unsteadiness the surface pressure fluctuations beneath the interaction produced by an unswept, sharp fin at 9° incidence were recorded. A Kulite LPS-125-IOM differential pressure transducer having a resonant frequency of 70 kHz was used. The four measuring stations are shown in (Fig. 22). Care was taken to ensure that the transducer diaphragm was flush with the surface since this is known to affect both the overall level of the power spectrum and the RMS value of the recorded signal.

The amplified pressure transducer output was recorded on tape before replaying into a Digital MINC minicomputer which was used to evaluate the RMS value of the fluctuating signal and the power spectral density of the signal.

Of the four positions shown in Fig. 22 the mean position of the separation, as indicated by the surface oil flow pictures, was just upstream of position III. The signal recorded at station I with the fin removed has a value of $(Prms/q_\infty)$ of 4.27×10^{-3}, which is typical of other measured values in flat plate turbulent boundary layer flows. Station I is at the start of the interaction region and the measured value of $(Prms/q_\infty)$ did not change when the fin was replaced. The mean values of the fluctating pressures at the four measuring stations are shown in Fig. 23. The largest value is recorded in the neighbourhood of the mean separation line and is usually associated with movement of the separation shock[11]. However, the maximum value recorded in the present tests is only about 1½ times the undisturbed value, which is far

lower than the peak values of about 12 and 8 measured in blunt fin and two-dimensional ramp flows respectively, as reported by Dolling, Murphy and Bogdonoff[11,12] at a Mach number of 2.95.

Although more transducer positions are needed to properly define the peak in the present experiment (see Fig. 23) our measurements do suggest that the sharp-fin-induced separation is probably steadier than the corresponding separations in blunt-fin and in ramp flows.

In order to determine whether the movement of separation was oscillatory the power spectra of the pressure signals were obtained using the Fast Fourier Transform technique. No dominant frequency was found in the range of 1 to 50 kHz.

IV Conclusions

Glancing interaction generated by a sharp unswept fin produces early separation on the side wall. A weak primary vortex is formed lying close to the wall. The upstream influence of the interaction is large and the 'inviscid' pressure rise is smeared out over many boundary layer thicknesses. The flow patterns, though complex are reasonably well understood.

The effect of sweep on a sharp-fin shock-generator is equivalent to a reduction of incidence. So far as glancing interaction is concerned the dominant factor is the inviscid shock strength.

Blunting the leading edge changes the local flow pattern dramatically. The bow shock causes separation on the sidewall in the form of a series of horse-shoe vortices which weaken as they move downstream. A characteristic double peak is formed in the pressure distribution on the side wall in the vicinity of the nose. For a blunt fin at incidence the nose region is bluntness dominated but the far field is incidence dominated and becomes similar to that for a sharp fin.

The effect of sweep on a blunt fin is highly beneficial since it effectively reduces both the nose radius and the effective incidence. Once again it is the inviscid shock strength that controls the interaction.

All the turbulent interactions studied were by definition unsteady, a condition masked by mean flow measurements. For the sharp fins used in our experiments the 'natural unsteadiness' of the turbulent flow was only increased by about 50% in the interaction region and no dominant frequency was found. For blunt fins the oil flow pictures suggest a higher amplification and measurements made elsewhere suggest a ten-fold increase in the pressure fluctuations.

V References

1. Settles, G.S. and Dolling, D.S. Swept shock wave/boundary layer interactions, to be published in "Tactical missile aerodynamics" by the AIAA, (late 1986)

2. Kubota, H. and Stollery J.L. An experimental study of the interaction between a glancing shock wave and a turbulent boundary layer. J. Fluid Mech. Vol. 116 pp 431-458 (1982).

3. Elfstrom, G.M. Turbulent hypersonic flow at a wedge-compression corner. J. Fluid Mech. Vol. 53 pp 113-127 (1972).

4. Settles, G.S. and Lu, F.K. Conical similarity of shock/boundary-layer interactions generated by swept and unswept fins. AIAA Jnl. Vol. 23 July (1985).

5. Shen, P.S. Three dimensional flow separation of a plane incompressible laminar boundary layer caused by a half-delta wing on a flat plate. NRC Canada Aero Rpt. LR-471 (1967).

6. Bertram, M.H., Feller, W.V. and Dunavant, J.C. Flowfields, pressure distributions and heat transfer for delta wings at hypersonic speeds. NASA TM X-316 (1960).

7. Stollery, J.L. and Richards, I.C. Supersonic flow past a slender delta wing - an experimental study. 10th Congress of ICAS. Paper No. 76-24 (1976).

8. Thwaites, B.(Ed) "Incompressible Aerodynamics" Oxford University Press (1960).

9. Winkelmann, A.E. Aerodynamic interaction phenomenon produced by a protuberance partially immersed in a turbulent boundary layer at Mach 5. AGARD CP71-71 (1970).

10. Fomison, N.R. PhD thesis. Cranfield Institute of Technology (1986).

11. Dolling, D.S. and Bogdonoff, S.M. An experimental investigation of unsteady behaviour of blunt fin induced shock wave/turbulent boundary layer interactions. AIAA paper 81-0336 (1981).

12. Dolling, D.S. and Murphy, M. Wall pressure fluctuations in a supersonic separated compression ramp flowfield. AIAA paper 82-0986 (1982)

VI Notation

$A_{1,2,3,..}$	attachment lines
CC	complete convergence
D	leading edge diameter measured normal to the edge
IC	incomplete convergence
M	Mach number
P	pressure
Re	Reynolds number
$S_{1,2,3,..}$	separation lines
X Y Z	Co-ordinate system defined on figures
α	incidence
δ	99.5% boundary layer thickness
Θ	shock wave angle
Λ	leading edge sweep
μ	Mach angle

Subscripts

g,s,gs	as used on X,Y and Z, see individual figs.
i	incipient
o	total
rms	root mean square
∞	freestream
δ	99.5% boundary layer thickness

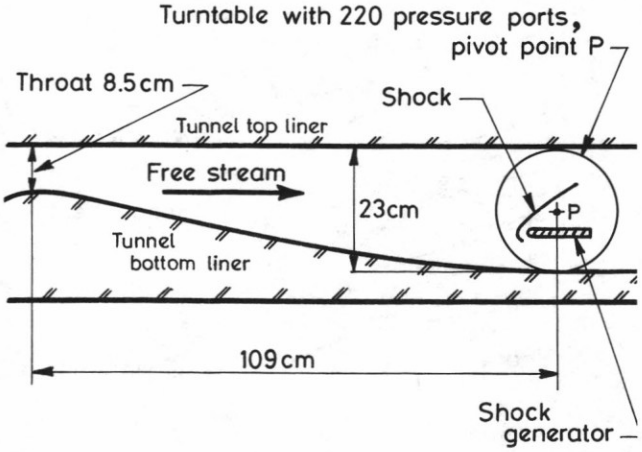

Figure 1. Experimental arrangement in the 23cm x 23cm wind tunnel.

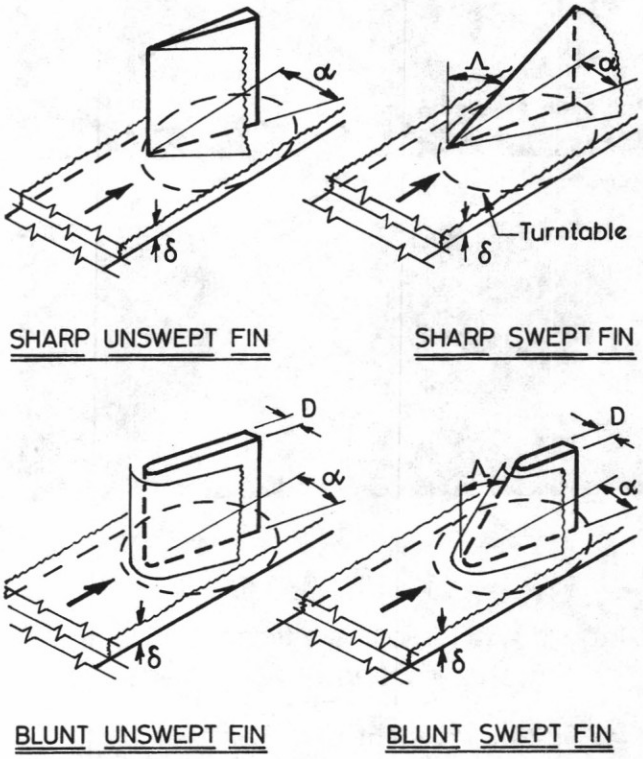

Figure 2.a. Configurations tested.

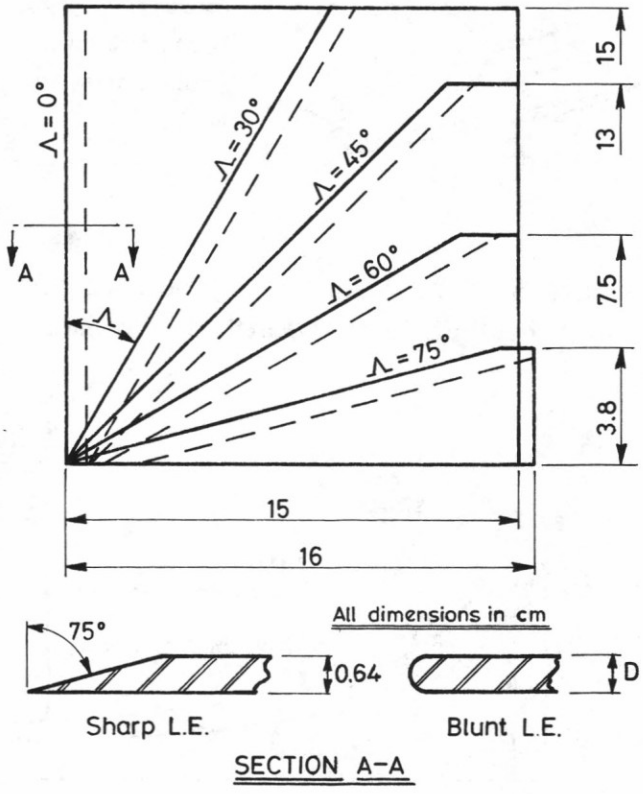

Figure 2.b. The shock generators tested.

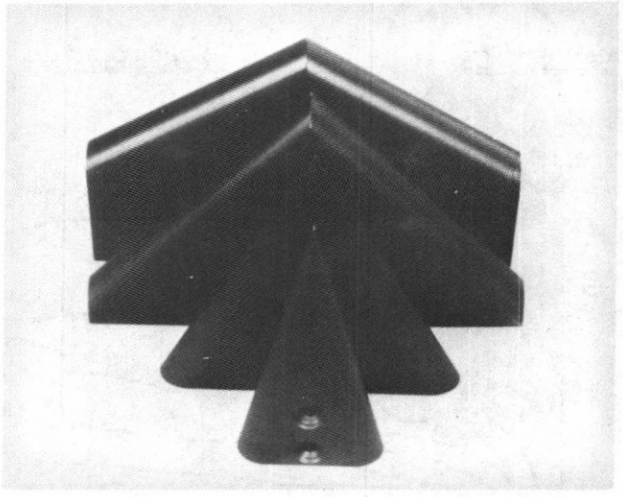

Figure 3. A typical set of delta models, Λ = 30°, D = 2.5cm.

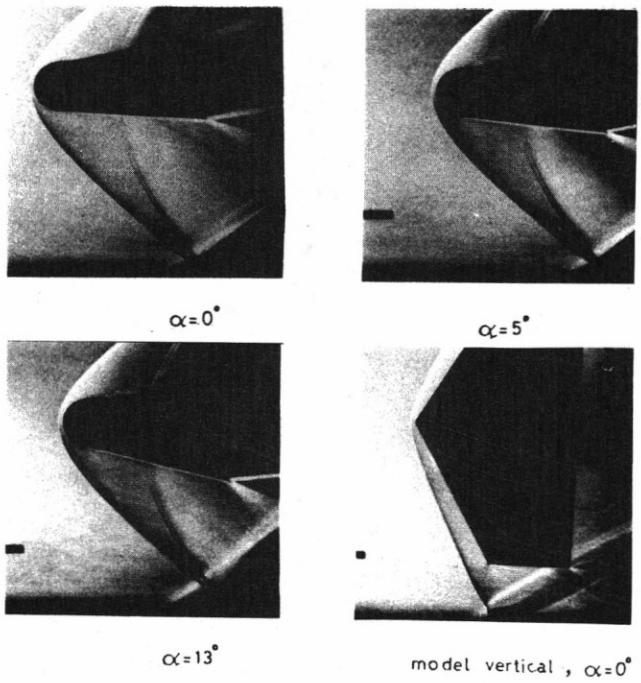

$\Lambda = 30°$ D = 2·5cm.

Figure 4. Typical schlieren pictures of the inviscid shock waves.

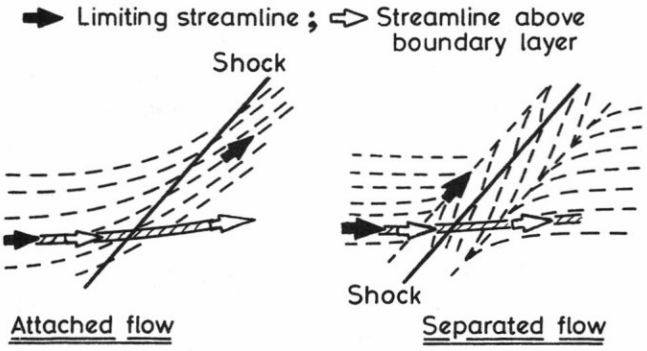

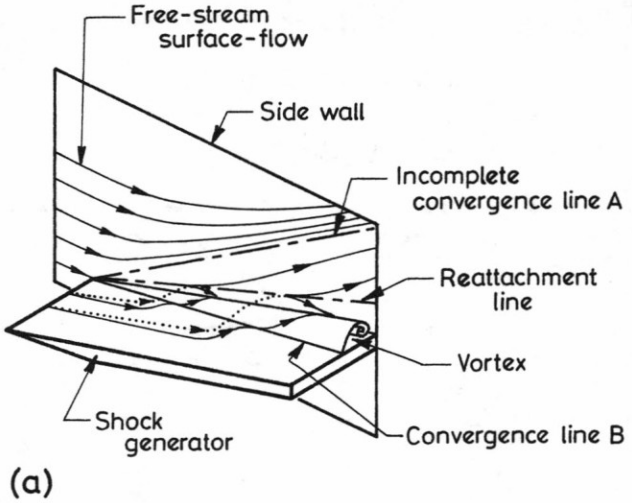

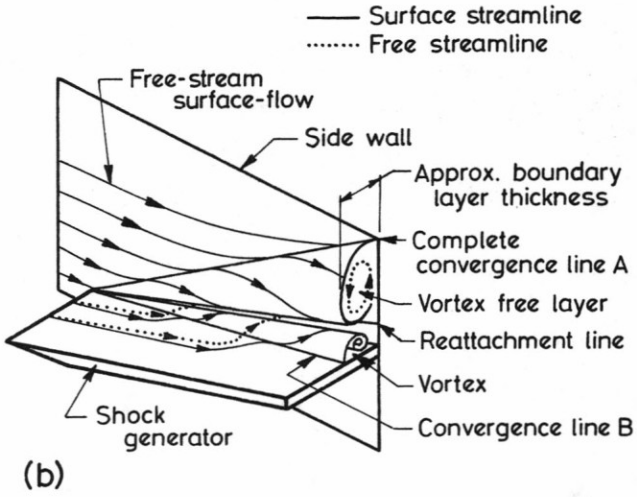

Figure 5. Streamlines in: (a) the attached flow field ; (b) the separated flow field.

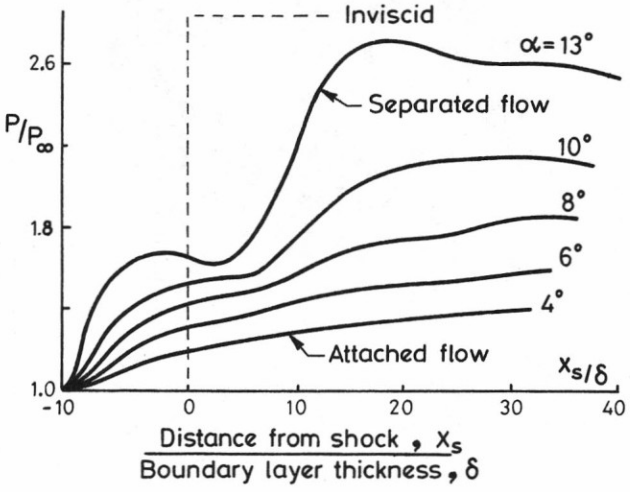

Figure 6. Glancing interaction.

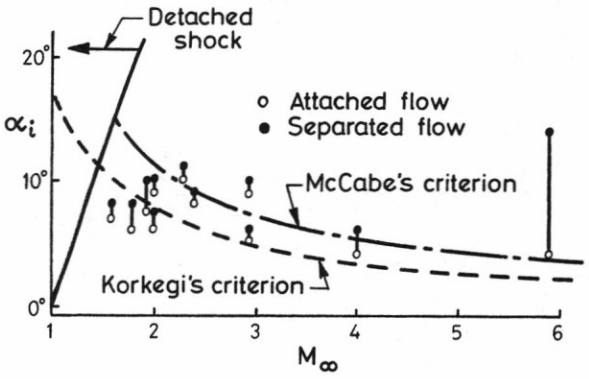

Figure 7. Shock-generator angle to induce incipient separation defined by complete oil-flow convergence. Taken from ref.2.

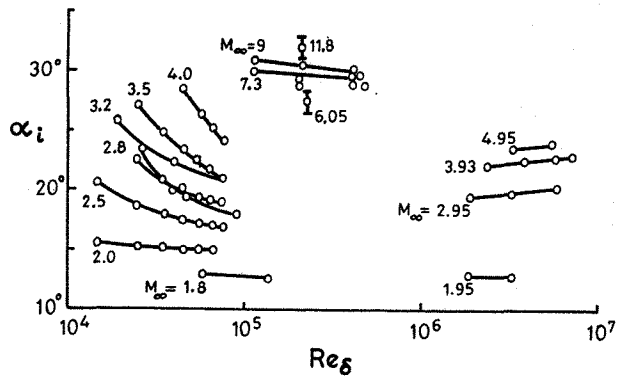

Figure 8. Incipient separation at a wedge compression corner. Taken from ref. 3.

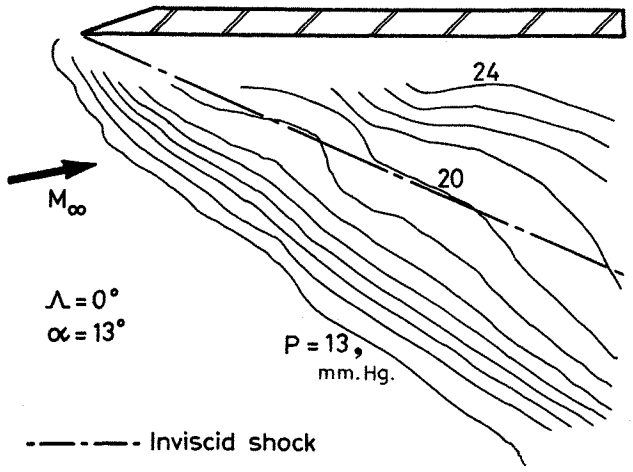

Figure 10.a. Sidewall isobars.

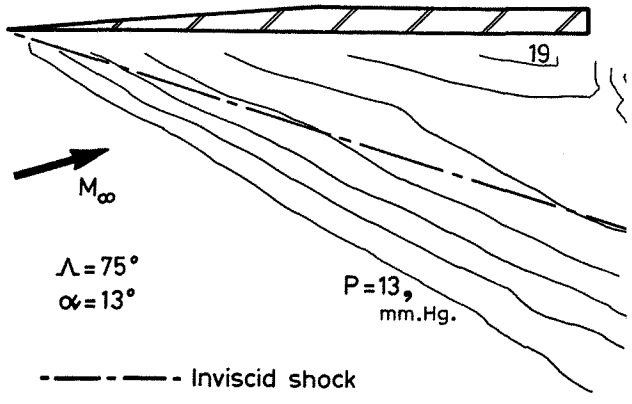

Figure 10.b. Sidewall isobars.

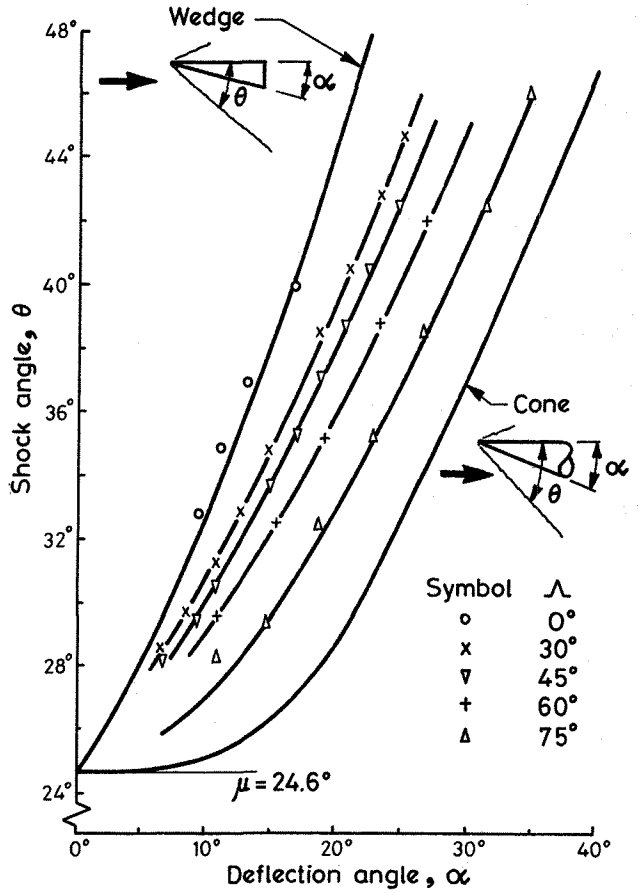

Figure 9. Delta wing centreline shockwave angles.

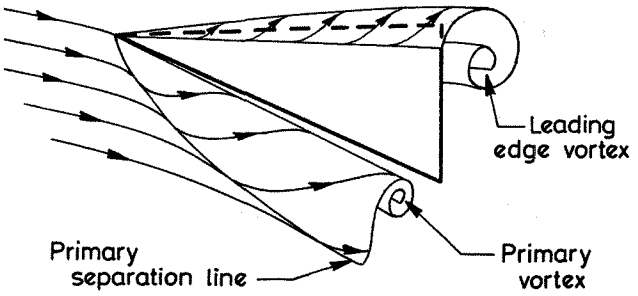

Figure 11. Flowfield produced by a half-delta wing vortex generator according to Shen (1967), ref.5.

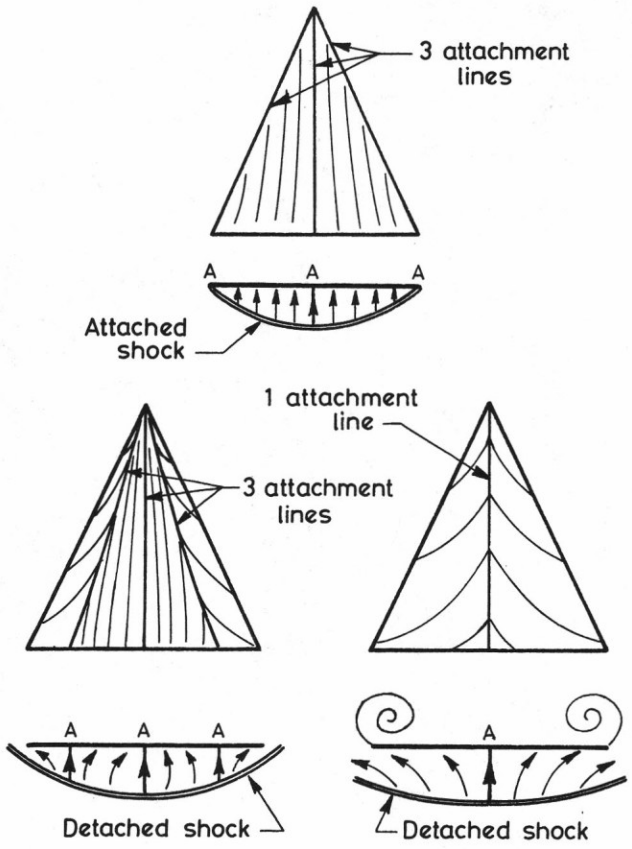

Figure 12. Types of flow on the windward side of a delta wing at incidence.

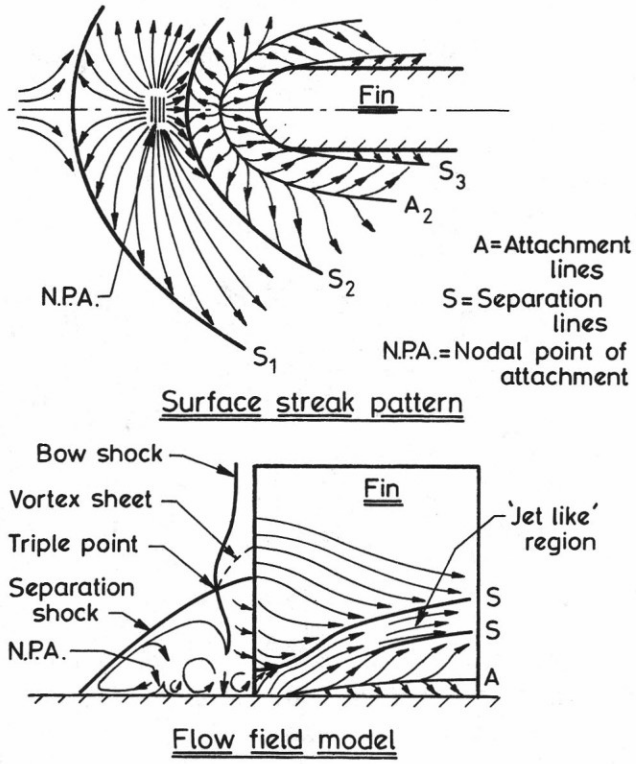

Figure 14. Winklemann's flow field model for unswept blunt fin interaction, ref. 9.

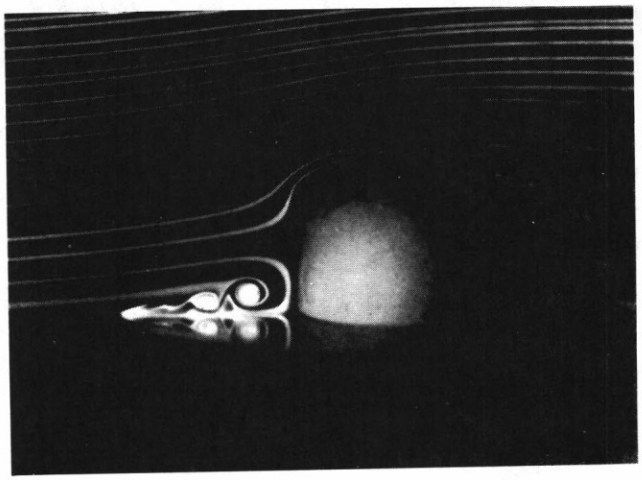

Figure 13. Low speed smoke flow about obstacle, ref. 8.

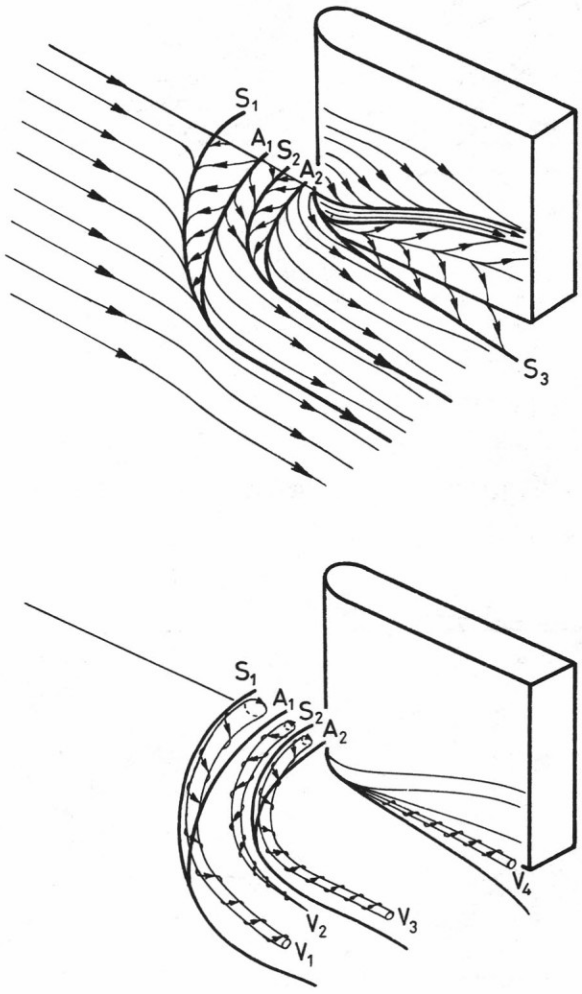

Figure 15. Flow around a blunt fin. $\Lambda = 0°$, $\alpha = 0$.

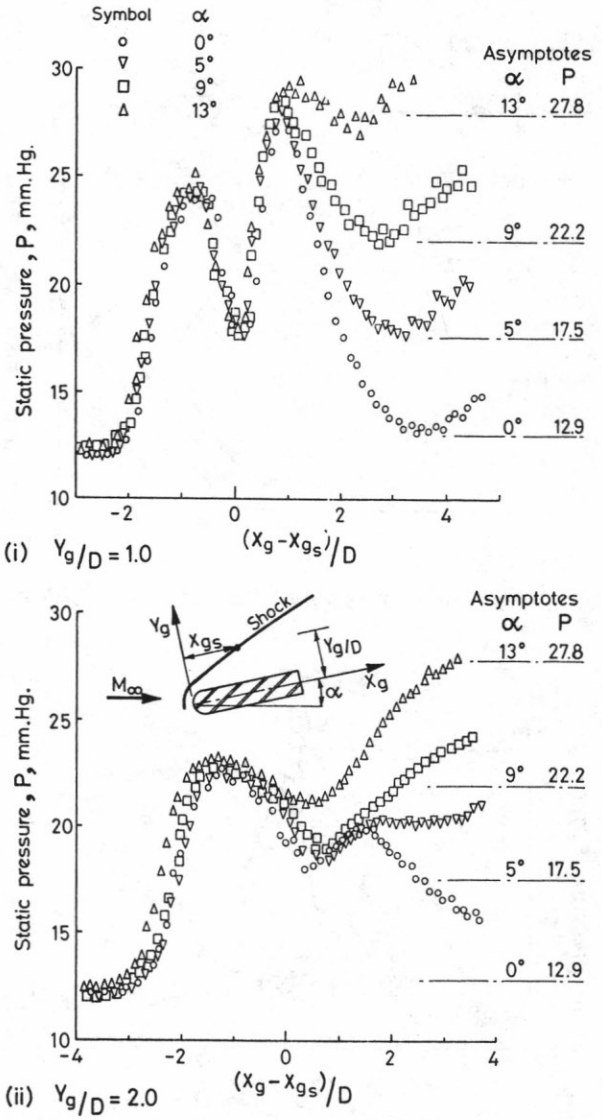

Figure 16.a. Incidence effect on the surface pressure distribution, $\Lambda = 0°$, D = 2.5 cm.

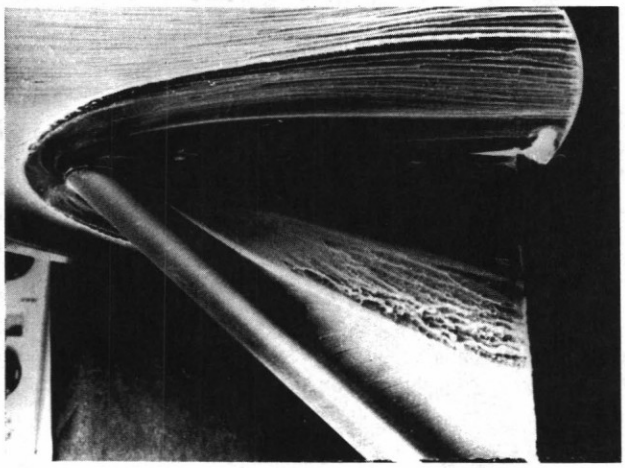

Figure 18. Oil-flow pattern, $\Lambda = 45°$, $\alpha = 0°$, D = 2.5 cm.

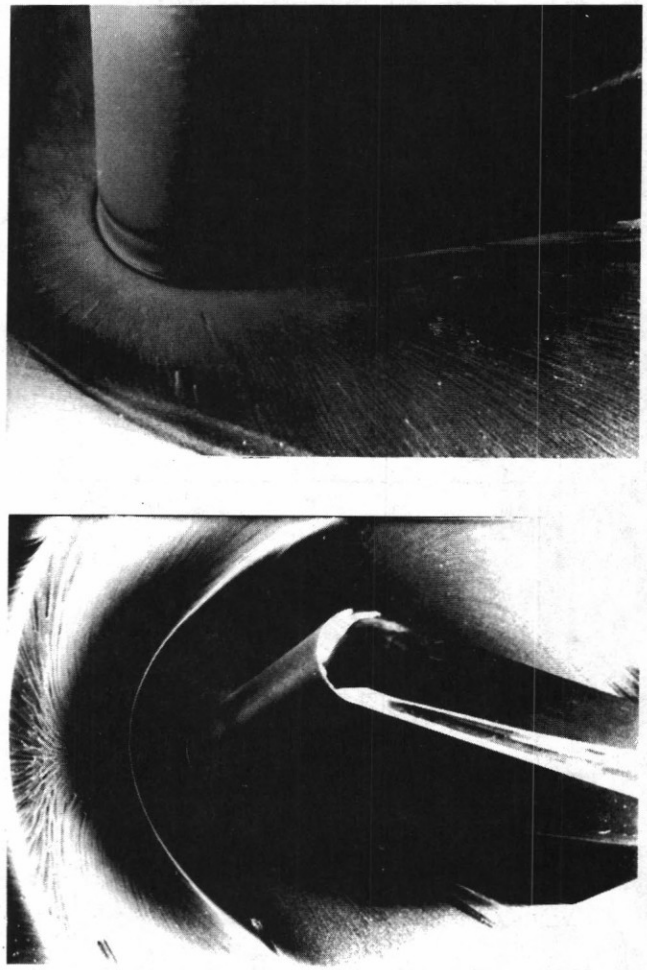

Figure 16.b. Blunt unswept wing, $\alpha = 15°$, D = 2.5 cm.

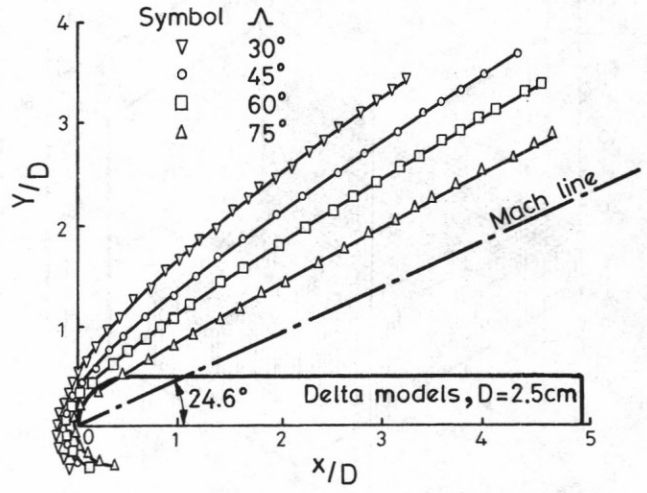

Figure 17. Effect of leading edge sweep angle on the shock profile, $\alpha = 0°$, D = 2.5 cm.

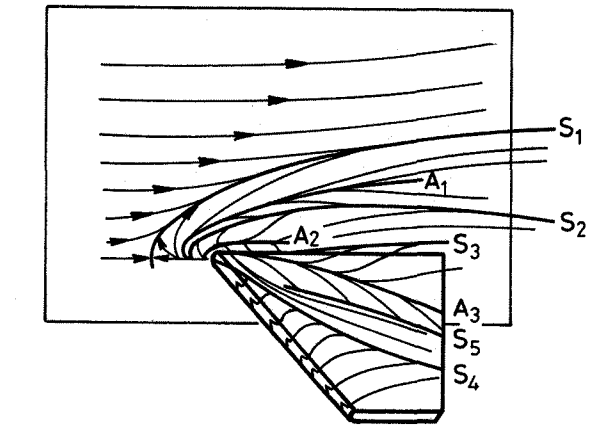

Surface streak pattern

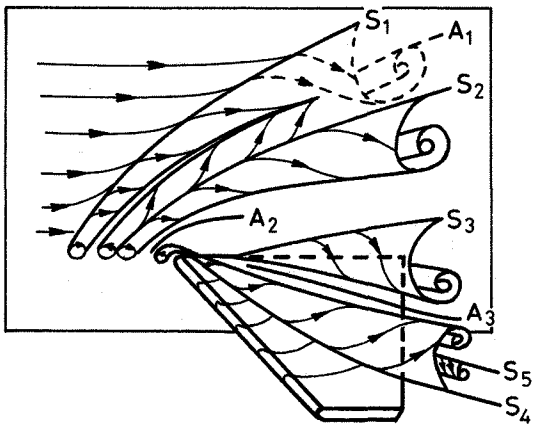

Vortex skeleton representation

Figure 19. Flow field model for blunt swept fins, $\Lambda = 45°$, $\alpha = 0°$, D = 2.5 cm.

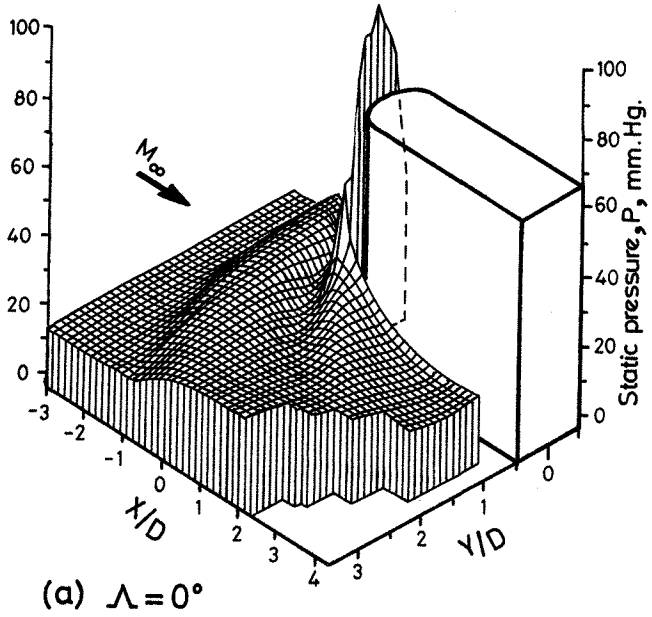

(a) $\Lambda = 0°$

Figure 21. Static pressure distributions, $\alpha = 0°$, D = 2.5 cm.

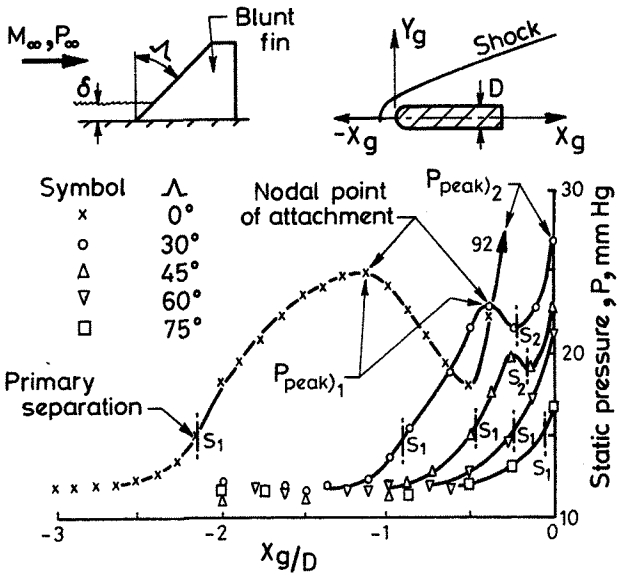

(a) Centre line pressure distribution, $Y_{g/D} = 0$

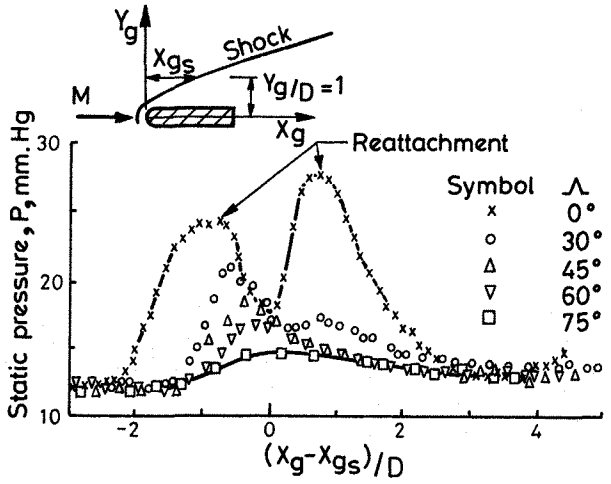

(b) Pressure distribution, $Y_{g/D} = 1$.

Figure 20. Effect of leading edge sweep angle on the surface pressure distribution $\alpha = 0°$, D = 2.5 cm.

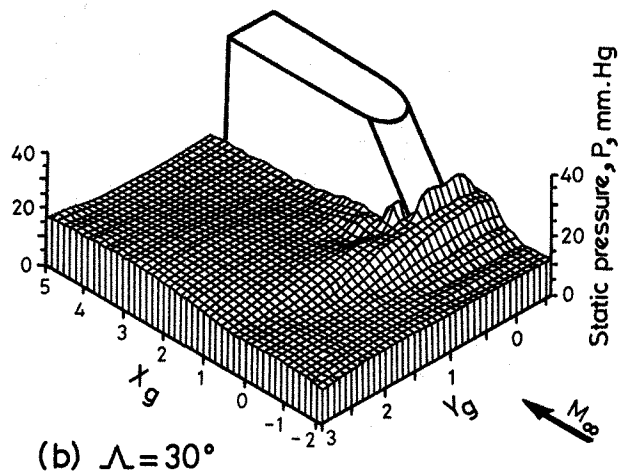

(b) $\Lambda = 30°$

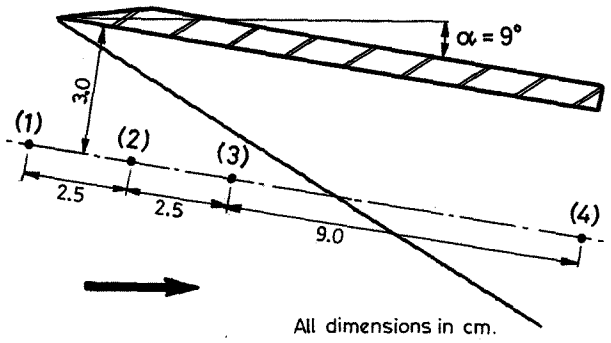

Figure 22. Transducer positions for unsteady pressure measurements.

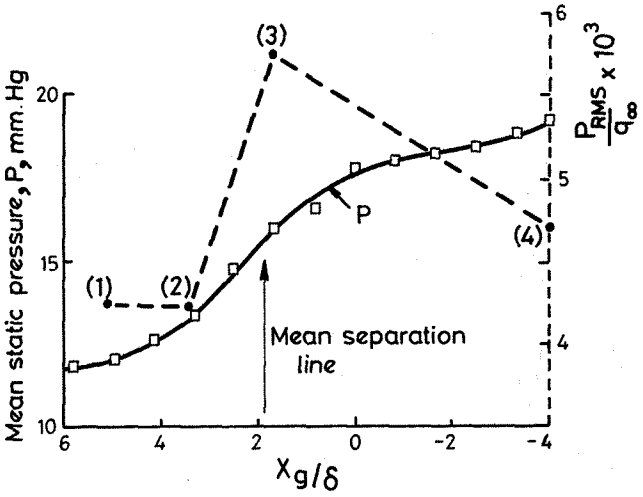

Figure 23. Mean static pressures and RMS values of the pressure fluctuations, $\Lambda = 0°$, $\alpha = 9°$, $Y = 3.2\,cm$, $D = 0$.